AGU ADVANCING EARTH AND SPACE SCIENCE

Geophysical Research Letters®

RESEARCH LETTER
10.1029/2022GL100233

Key Points:

- We build a 3-D high-resolution upper to middle crust azimuthally anisotropic model of southern California using local *P*-wave arrival times
- Present anisotropy mostly reflects shape preferred orientation of stress-related microcracks in the shallow crust and crystallographic preferred orientation of paleo mineral fabrics at larger depths
- Distinct anisotropy beneath the western Transverse Ranges from its adjacent blocks reflects its history with rotation up to 110°

Supporting Information:

Supporting Information may be found in the online version of this article.

Correspondence to:

P. Tong,
tongping@ntu.edu.sg

Citation:

Wu, S., Jiang, C., Schulte-Pelkum, V., & Tong, P. (2022). Complex patterns of past and ongoing crustal deformations in Southern California revealed by seismic azimuthal anisotropy. *Geophysical Research Letters*, *49*, e2022GL100233. https://doi.org/10.1029/2022GL100233

Received 29 JUN 2022
Accepted 25 JUL 2022

Author Contributions:

Conceptualization: Shucheng Wu, Ping Tong
Formal analysis: Shucheng Wu
Funding acquisition: Ping Tong
Investigation: Shucheng Wu
Methodology: Ping Tong
Supervision: Ping Tong
Validation: Chengxin Jiang, Vera Schulte-Pelkum
Visualization: Shucheng Wu
Writing – original draft: Shucheng Wu
Writing – review & editing: Chengxin Jiang, Vera Schulte-Pelkum, Ping Tong

Complex Patterns of Past and Ongoing Crustal Deformations in Southern California Revealed by Seismic Azimuthal Anisotropy

Shucheng Wu[1,2], Chengxin Jiang[3], Vera Schulte-Pelkum[4], and Ping Tong[1,2,5]

[1]Division of Mathematical Sciences, School of Physical and Mathematical Sciences, Nanyang Technological University, Singapore, Singapore, [2]Earth Observatory of Singapore, Nanyang Technological University, Singapore, Singapore, [3]Research School of Earth Science, The Australian National University, Canberra, ACT, Australia, [4]Cooperative Institute for Research in Environmental Sciences and Department of Geological Sciences, University of Colorado Boulder, Boulder, CO, USA, [5]Asian School of the Environment, Nanyang Technological University, Singapore, Singapore

Abstract We present a high-resolution *P*-wave azimuthally anisotropic velocity model for the upper and middle crust beneath southern California by a novel adjoint-state traveltime tomography technique. Our model reveals significant anisotropy variations between tectonic blocks that clearly reflect both past and current plate boundary deformation. In the shallow crust, seismic anisotropy is mostly controlled by the preferred alignment of microcracks related to the present N-S compressive stress; while at deeper depths (>~6 km), seismic anisotropy mainly records paleofabrics formed during the long-lived Farallon subduction and later extension that have not been fully reset by the present transform motion. Interestingly, our model demonstrates distinct fast axes beneath the western Transverse Ranges from its neighboring blocks, probably reflecting the large-scale vertical axis clockwise rotation of the block. In addition, we identify layered structures with distinct anisotropy features beneath the Salton Trough, which could be a result of the current transtension.

Plain Language Summary Seismic anisotropy, which is defined as the directional dependence of the speed of seismic waves in a rock matrix, provides important constraints on the dynamic processes of the Earth. Here, we investigate this parameter in the upper to middle crust beneath southern California where the Pacific Plate slides northwestward with respect to the North American Plate by a novel seismic imaging technique. We find that present crustal anisotropy in southern California reflects both the past and current plate boundary deformation. While the shallow crustal anisotropy is dominantly controlled by the present stress, seismic anisotropy at larger depths (>~6 km) mainly reflects paleofabrics associated with Mesozoic subduction and later extension. The clockwise rotation of the western Transverse Ranges is clearly resolved by its distinct anisotropy as compared to its neighboring blocks. On the other hand, we show that seismic anisotropy beneath the Salton Trough may be fully controlled by the current deformation, forming layered structures with distinct anisotropy features.

1. Introduction

Southern California represents a complex segment of the transform plate boundary between the North American and Pacific plate (Figure 1a), having experienced a transition from the long-lived Mesozoic subduction to later extensional and transform tectonic regimes (Atwater, 1970). Such a transition has resulted in significant crustal deformation represented by a series of crustal block fragmentation, microplate capture, lateral movement, and vertical axis rotation in this region, in particular to the west of the San Andreas Fault (SAF) (e.g., McQuarrie & Wernicke, 2005). Tectonic reconstructions revealed that blocks west of the SAF were a once-continuous magmatic arc that was later disaggregated by the transform motion (Saleeby, 2003). In addition to long distance translations of the crustal blocks west of the SAF, the western Transverse Ranges (WTR) showed a notable up to 110° clockwise rotation (e.g., Nicholson et al., 1994). The associated in-land jump of the transform plate boundary and rifting in the Gulf of California have led to the development of oblique extension in the Salton Trough (ST) since ~6 Ma, which completes the tectonic reorganization west of the SAF (McQuarrie & Wernicke, 2005). To the east of the SAF, crustal deformation is dominated by mid-Tertiary extension and later right-lateral shear in the Mojave Desert, in comparison to a nearly undeformed rigid Sierra Nevada block in the north (Dokka &

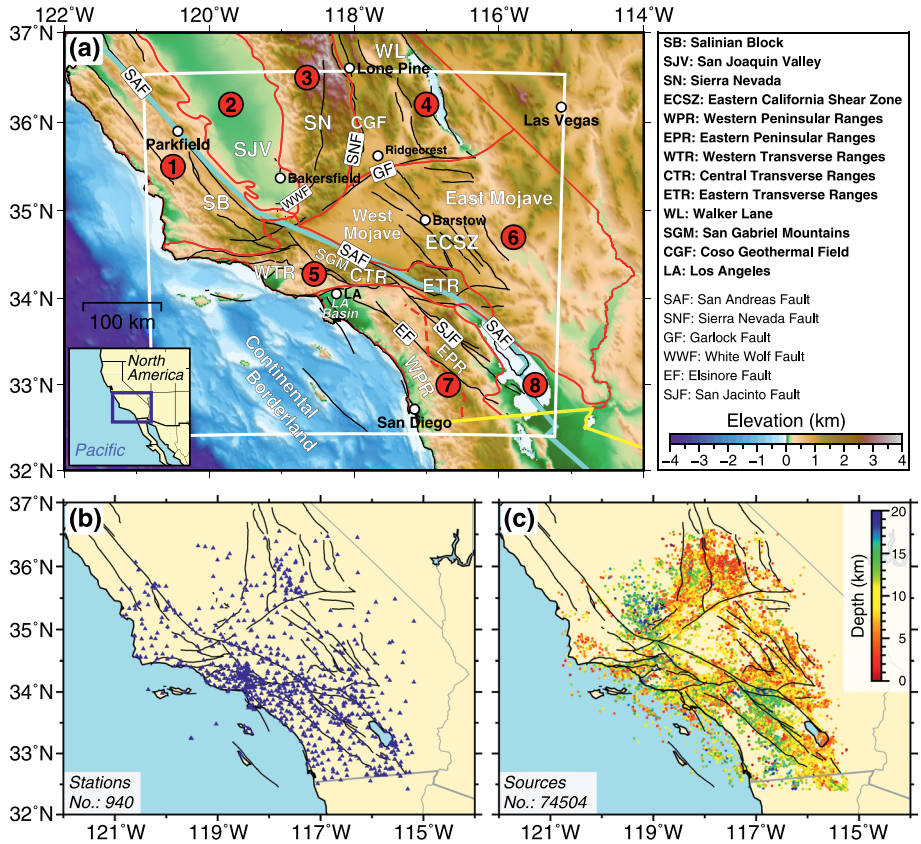

Figure 1. (a) Location and topography of southern California overlaid with geologic and tectonic features. The red lines separate major tectonic blocks: 1. Coast Ranges, 2. Great Valley, 3. Sierra Nevada, 4. Basin and Range, 5. Transverse Ranges, 6. Mojave Desert, 7. Peninsular Ranges, and 8. Salton Trough. The black, yellow, and cyan lines represent major faults (Jennings, 1994), national borders, and plate boundary (Bird, 2003), respectively. The white box outlines the study region with location shown in the inset. The distributions of selected seismic stations and earthquake sources are shown in (b and c), respectively.

Travis, 1990). All the past and ongoing deformation should have left an imprint on the present-day crustal structure, leaving footprints that can be captured by seismic anisotropy tomography.

Seismic anisotropy is a strong indicator of dynamic processes inside the Earth, produced by the preferred alignment of mineral fabrics and/or microcracks that are difficult to resolve by isotropic velocity models. Compared to the many isotropic models that generally agree with each other, the limited number of anisotropic studies in southern California exhibit complex anisotropy at different depths. For instance, local shear-wave splitting (SWS) analyses showed complex anisotropic patterns simultaneously controlled by stress and local structures (Boness & Zoback, 2006; Li & Peng, 2017). Meanwhile, receiver function azimuthal harmonic analyses highlighted pervasive inherited anisotropic features in the crust that are possibly related to past deformation (Porter et al., 2011; Schulte-Pelkum et al., 2020). Recently, by analyzing all the available anisotropy indicators, Schulte-Pelkum et al. (2021) further concluded that the current anisotropy in the lithosphere of southern California preserves fabrics/structures formed during the long-lived Mesozoic subduction and later extension that have not been reset by the present transform tectonic regime. However, the model of Schulte-Pelkum et al. (2021) in the seismogenic crust relies heavily on SWS results that are more sensitive to local structures with limited vertical resolution (Savage, 1999; Zhao et al., 2016). Furthermore, regional surface wave azimuthally anisotropic inversions only map anisotropy with respect to period (Lin et al., 2009; Zigone et al., 2015), producing highly variable results at different periods and lateral locations that are hard to interpret. As a result, the lack of high-resolution 3-D azimuthally anisotropic models for the crust of southern California inhibits our understanding of how plate boundary deformation is accommodated in the crust.

In this study, we attempt to constrain crustal azimuthal anisotropy in southern California using a massive number of local *P*-wave arrival times accumulated in the past 40 years. This is technically challenging since ray tracing in anisotropic media is rather complex, especially in the highly heterogeneous crust (e.g., Wang, 2014). Here, we solve this problem by using a new adjoint-state traveltime tomography technique that requires no ray tracing (Tong, 2021). *P*-wave propagation and model reconstruction are achieved by solving the azimuthally anisotropic eikonal equation with a highly reliable numerical algorithm and the associated optimization problem with the efficient adjoint-state method. Importantly, the adjoint-state traveltime tomography method can precisely compute the sensitivity kernels with respect to *P*-wave slowness and azimuthal anisotropy even in very complex media (Tong, 2021). The combination of the abundant data and advanced method allows us to reliably constrain crustal velocity heterogeneities and azimuthal anisotropies at unprecedented resolution, which provides new insights toward understanding the deformation and dynamics in the Pacific-North America plate boundary region.

2. Data and Methods

2.1. First *P*-Wave Arrival Times

We use first *P*-wave arrival times spanning from 1981 to 2021 archived in the Southern California Earthquake Data Center (SCEDC, 2013). We only consider arrivals with high signal onset quality from earthquakes with magnitude greater than 1.5 and focal depth shallower than 20 km. We remove the arrivals with epicenter distance greater than 120 km to separate Moho refractions (Pn waves) from our data set. Then, we discard clustered data by dividing the research region into 1 km × 1 km × 0.5 km blocks and only keep one earthquake in each block based on the largest number of available arrivals. We further require that each station must record at least eight arrivals, and each arrival must be recorded by at least eight stations. Finally, we adjust the hypocenter locations according to the waveform relocated HYS_catalog_2011 (extended to 2019) of Hauksson et al. (2012) and delete earthquakes not included in the relocated catalog. As a result, a total of 1,509,004 high-quality first *P*-wave arrivals from 74,504 local earthquakes are selected for the subsequent tomographic inversions (Figures 1b and 1c).

2.2. Adjoint-State Traveltime Tomography

We employ the adjoint-state traveltime tomography method for azimuthally anisotropic media (Tong, 2021) to iteratively invert for *P*-wave velocity and azimuthal anisotropy (magnitude and fast velocity orientation). In the forward calculation, we set up a fine 3-D forward grid with a size of 1 km × 1 km × 0.5 km and numerically solve the anisotropic eikonal equation using a fast-sweeping method (Qian et al., 2007). Sensitivity kernels of the objective function with respect to the *P*-wave slowness and anisotropic parameters are calculated based on the traveltime field and an adjoint field that satisfies the transport-type adjoint equation (Tong, 2021). The inverse problem is handled by a step-size-controlled gradient descent method that requires the relative perturbations not to exceed ±2% at each iteration. Note that we apply a multiple-grid model parameterization comprising 8 sets of staggered grids in the inversion, which naturally acts as a smoothing term. The multiple-grid setup is also demonstrated to have a better performance in capturing subsurface heterogeneities than a conventional collocated grid (Tong et al., 2019). We use different inversion grid sizes for the *P*-wave slowness and anisotropic parameters, as determining the anisotropy generally requires a better data azimuthal coverage (e.g., Yu & Zhao, 2018). Therefore, the horizontal spacing of the inversion grid is two times larger for the anisotropic parameters than that designed for the *P*-wave slowness.

The inversion starts with a 3-D isotropic *P*-wave velocity model of Wu et al. (2022), which is a high-resolution crustal velocity model built from jointly inverting arrival times of first *P*-wave and high-quality Moho reflected PmP waves. We also perform an inversion using a 1-D starting model, that is, the 1-D HK model (Hadley & Kanamori, 1977) with a smoothed transition between layers and an undulating Moho surface of Tape et al. (2012). The resulting velocity and anisotropic patterns show minor differences to those obtained from the 3-D starting model (Figures S1 and S2 in Supporting Information S1). We here choose to start with the 3-D velocity model because it is constrained by two different types of data and produces much smaller data residuals. The tomographic scheme involves three steps. We first perform 40 iterations to generate an anisotropic velocity model for earthquake relocation. Then, we relocate all 74,504 earthquakes with 10 iterations following the algorithm described in Tong (2021) and update the associated *P*-wave arrival times. Finally, starting again with the 3-D isotropic velocity model, we conduct another 40 iterations using the relocated earthquakes to construct our final

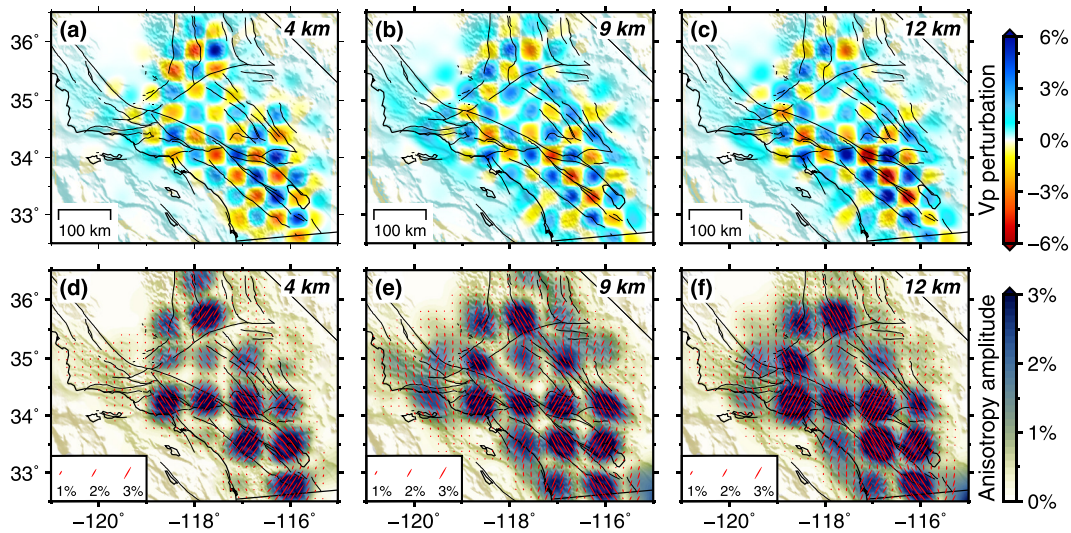

Figure 2. The results of the checkerboard resolution test for average *P*-wave velocity (a–c) and azimuthal anisotropy (d–f) at three example depths. The red bars in (d–f) represent fast *P*-wave orientations. The black lines denote major faults in the region.

model. During the tomographic inversion, data with either large absolute traveltime misfit ($|T_{obs} - T_{pred}| > 5$ s) or large relative traveltime misfit ($|T_{obs}/T_{pred} - 1| > 0.5$) are removed. In the three-step inversion, we achieve data misfit reductions of ∼13%, ∼59%, and ∼27%, respectively.

3. Results

We first conduct several checkerboard tests to assess the resolving ability of our data and the robustness of the tomographic inversion, including one test simultaneously incorporating velocity and anisotropic anomalies and two additional tests incorporating either velocity or anisotropic anomalies for trade-off analysis. The input velocity and anisotropic anomalies are designed based on sinusoidal functions following Tong (2021). Details of the checkerboard resolution tests are given in (Text S1 of Supporting Information S1). In general, these checkerboard resolution tests show a satisfactory recovery of 40-km-wide velocity and 80-km-wide anisotropy anomalies (Figure 2; Figures S3 and S4 in Supporting Information S1), albeit with recovered amplitudes beneath the Mojave Desert and fringe regions that are slightly under-estimated due to sparser data coverage there. The resolution at depths greater than 16 km is also low as we exclude earthquakes below 20 km depth and Pn arrivals from our data set. In particular, the two additional checkerboard tests indicate that the velocity and anisotropic parameters seem to be mostly decoupled (Figures S5–S8 in Supporting Information S1), thanks to the abundant and almost evenly distributed data in southern California (Figures 1b and 1c).

3.1. Average *P*-Wave Velocity

The inverted 3-D average *P*-wave velocity model is consistent with most previous regional velocity models (e.g., Lee et al., 2014; Shaw et al., 2015; Tape et al., 2009). Shallow velocity structures match well with surface geology, with low velocities dominating major sedimentary basins and high velocities beneath regions where batholitic rocks are exposed (Figure 3a). Meanwhile, clear velocity contrasts are resolved across major strike-slip faults, such as the SAF, Garlock Fault (GF), San Jacinto Fault (SJF), and Elsinore Fault (EF) (Figure 3), indicating potentially prominent lithological changes across the faults (e.g., Berg et al., 2018). In the middle to lower crust (>10 km), velocity anomalies can be generally explained by different rock compositions and/or presence of fluids (e.g., Barak et al., 2015; Berg et al., 2018; Han et al., 2016; Nicholson et al., 1994; Tape et al., 2009). Since most of the velocity anomalies have been discussed thoroughly in many previous studies, we will focus on the less explored azimuthal anisotropy hereafter.

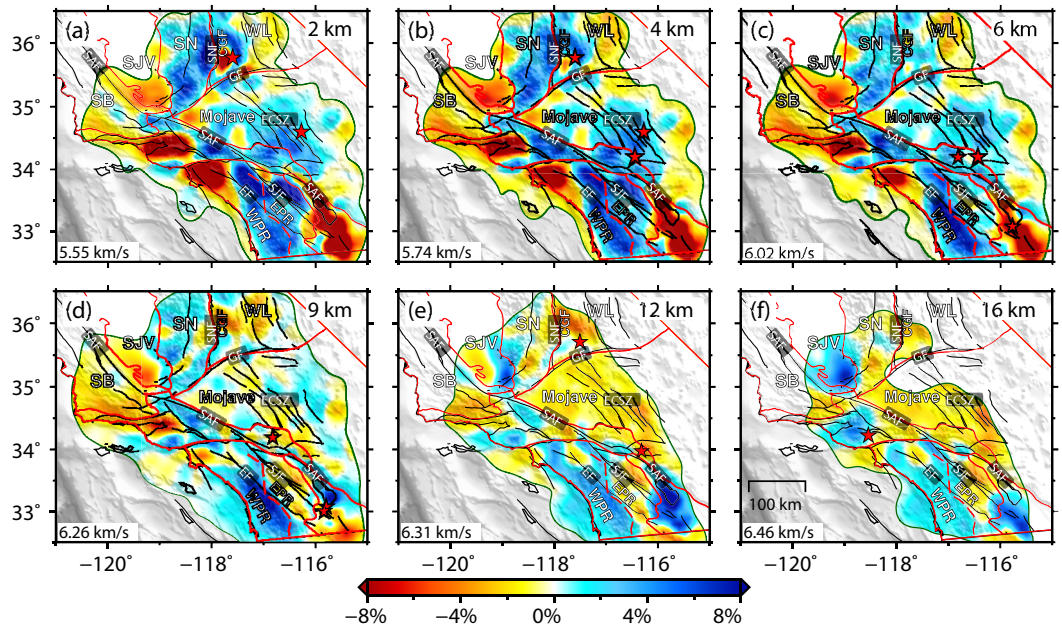

Figure 3. *P*-wave velocity perturbations at six representative depths. The reference *P*-wave velocity for each depth slice is given at the bottom left corner. Abbreviations and symbols are the same as Figure 1. Major earthquakes with magnitude larger than 6.0 are denoted by red stars.

3.2. Azimuthal Anisotropy

Our new model reveals significant 3-D anisotropic variations (Figure 4) in the crust of southern California that have not been discussed in detail before. North of the GF, fast *P*-wave velocity orientations are generally N-S aligned, with an exception near the Coso geothermal field where clear rotations of the fast axes to E-W are observed (Figures 4a–4d). This pattern agrees well with a previous smaller-scale tomographic study which suggests a clockwise rotating crustal block associated with fluids that have possibly led to the nucleation of the 2019 Ridgecrest earthquake (Tong et al., 2021). The Mojave Desert shows nearly uniform NE-SW fast orientations, with the eastern Mojave Desert exhibiting larger anisotropy amplitudes as compared to the west (Figures 4a–4c). Interestingly, small patches of weak NW-SE oriented fast axes are found in the southernmost Eastern California Shear Zone (ECSZ) in the shallow crust (Figure 4b), consistent with the spatial distribution of ongoing rock damage production beneath the ECSZ (Ben-Zion & Zaliapin, 2019). Therefore, the fault-parallel anisotropy likely reflects local structures created by earthquake rupture and shear, such as the presence of strike-parallel fluid-filled fractures and/or fault gouge (Boness & Zoback, 2006). Overall, the azimuthal anisotropy east of the SAF shows a relatively uniform pattern with a few local variations.

To the west of the SAF, however, significant anisotropy variations can be found between different tectonic blocks. The most notable and intriguing feature is NE-SW oriented fast axes beneath the WTR, which are nearly perpendicular to the strike of the SAF. This fault-perpendicular fast orientation stands out from the generally fault-parallel fast axes (NW-SE) in the surrounding blocks, such as the Salinian block (SB) and the northern parts of the western Peninsular Ranges (WPR) beneath the Los Angeles Basin (Figure 4d). In the southern parts of the WPR near San Diego, we notice a slightly different anisotropic pattern, that is, the fast axes rotate from nearly fault-perpendicular in the shallow crust (<6 km) to fault-parallel in the middle crust. The north-south discrepancy within the WPR is also revealed in the surface wave azimuthally anisotropic maps at short period (Zigone et al., 2015) and could be attributed to compositional variations reflecting the internal structure of the Mesozoic magmatic arc (Bao et al., 2021). Meanwhile, the eastern Peninsular Ranges (EPR) display very different azimuthal anisotropy as compared to the WPR, showing mostly fault-parallel fast axes at shallow depths (Figures 4a–4c) while they become much more complex in the middle crust (Figures 4d–4e). Our model also reveals distinct anisotropic layers beneath the ST, with fast velocity orientations changing from nearly N-S in the shallow crust (<6 km), to NE-SW at ~9 km depth, and then to NW-SE at greater depths (>12 km).

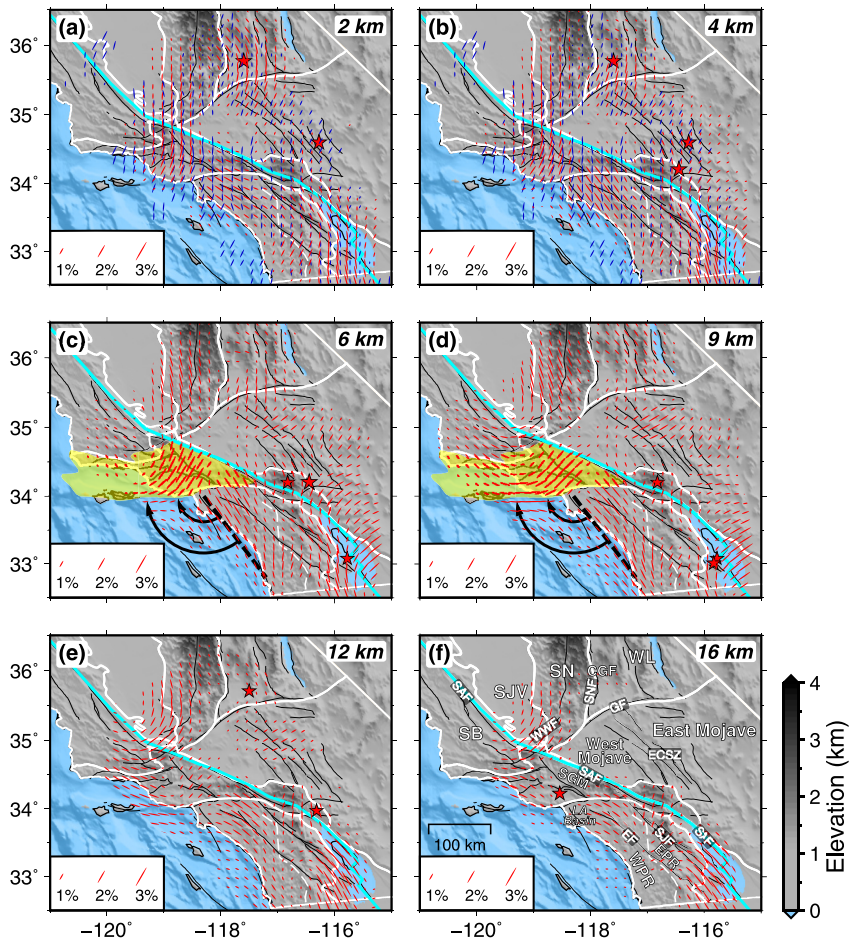

Figure 4. *P*-wave azimuthal anisotropy at six representative depths. The red bars denote the fast velocity orientations, while the blue bars represent the S_{Hmax} direction from Yang and Hauksson (2013). Yellow shaded area highlights blocks that have underwent significant vertical axis rotation (Hillhouse, 2010), with the restored fast axes prior to rotation shown as the black dashed line. The cyan line represents the present transform plate boundary from Bird (2003).

4. Discussion

4.1. Crack- and Mineral-Induced Anisotropy

Seismic anisotropy in the upper to middle crust is generally considered to be caused by the preferred orientation of microcracks and/or rock-forming minerals (e.g., Almqvist & Mainprice, 2017; Barruol & Mainprice, 1993; Crampin, 1987). The crack-induced anisotropy is often stress-related, produced by the shape preferred orientation (SPO) of microcracks under subcritical conditions (Boness & Zoback, 2006; Li & Peng, 2017). The resulting seismic anisotropy is large in amplitude with fast axes parallel to the maximum horizontal compressive stress ($S_{H\mathrm{max}}$) in regions away from major fault strands (Boness & Zoback, 2006). This type of anisotropy is typically confined to the very shallow crust with depths up to a few kilometers, as the increasing confining pressure leads to a pervasive closure of microcracks at depths (Porter et al., 2011; Rasolofosaon et al., 2000). However, exceptions may exist near deep-rooted fault zones, where crack-induced anisotropy is reported to dominate up to ~10 km depth (Audet, 2015). This scenario would require high-pressure (near-lithostatic) fluids to be sealed in a fracture network surrounded by impermeable country rocks. In our model, the lateral resolution is limited to tens of kilometers (Figure 2), meaning that fault-related cracks/fabrics (typically up to a few kilometers away from the fault strand) are difficult to resolve, unless a wide fracture network is maintained by a series of sub-parallel strike-slip faults like the ECSZ and the trifurcation area of the SJF.

Comparing our anisotropy results with the $S_{H\max}$ direction of Yang and Hauksson (2013), we find a largely consistent pattern at shallow crustal depths (<~6 km) east of the SAF (Figure 4a), revealing predominant crack-induced anisotropy related to the present N-S compression. While the shallow anisotropy to the west of the SAF also shows a general consistency, large deviations from $S_{H\max}$ can be found beneath the Los Angeles Basin and eastern parts of the San Gabriel Mountains (Figures 4a and 4b). This differs from previous SWS results which revealed generally stress-induced N-S aligned fast axes in the region (Li & Peng, 2017). Given the broad distribution of the fault-parallel anisotropy away from nearby major strike-slip faults (i.e., the SAF and EF), we invoke mineral-induced anisotropy to account for their misalignments with the stress orientation. This type of anisotropy is generated by the crystallographic preferred orientation (CPO) of anisotropic minerals formed during rock formation and subsequent deformation. The majority of minerals forming the continental crust show notable seismic anisotropy, such as the highly anisotropic mica and amphiboles, quartz, as well as the less studied feldspar family (Almqvist & Mainprice, 2017; Bernard & Behr, 2017). At middle crustal depths (>9 km), observed fast *P*-wave orientations deviate more from the $S_{H\max}$ direction, which could also be explained by a gradual transition from crack-to mineral-induced anisotropy with depth. For example, we find a small angle (10–20°) clockwise rotation of the fast axes from 2 to 12 km depth beneath the WTR and eastern Mojave, as well as more prominent deviations from the $S_{H\max}$ direction with depth beneath the ST and WPR near San Diego (Figure 4). We attribute the formation of the various CPOs to the past and ongoing deformation in the region, as discussed in more detail in the following section.

4.2. Past and Ongoing Deformation in Controlling the Seismic Anisotropy

There is a growing body of evidence addressing the important contribution of paleofabrics on the present-day anisotropy beneath southern California, mostly in the lower crust and lithospheric mantle (e.g., Audet, 2015; Porter et al., 2011; Schulte-Pelkum et al., 2020; Wang et al., 2020). However, it is unclear whether the inherited structures still exist in the upper and middle crust, as previous anisotropic models have relatively poor resolution at these depths.

Our model successfully fills in the resolution gap and shows distinct fast axes in the highly rotated WTR compared to the adjacent blocks (Figure 4c), strongly indicating the preservation of paleofabrics in the middle crust. Those inherited fabrics were formed during the long-lived Farallon subduction (accretion and intrusion) and subsequent extension and have not been reset by the present transform tectonic regime (Schulte-Pelkum et al., 2021). Assuming that paleofabric foliations formed during Farallon subduction stay perpendicular to the former NE convergent direction (thus nearly parallel to the strike of the present SAF) with intermediate to high dipping angles (Porter et al., 2011; Schulte-Pelkum et al., 2021), our model west of the SAF clearly delineates a pronounced anisotropic pattern in the WTR that is likely associated with the clockwise rotation. The once fault-parallel fast axes, formed as a result of compression, accretion, and intrusion during Farallon subduction, have been rotated subsequently to the current fault-perpendicular direction. We therefore suggest that the present seismic anisotropy at middle crustal depths may more likely represent CPO of paleo mineral fabrics that survived the overprinting process of the current transform motion. If this is the case, the fast axis angular difference between the rotated and unrotated adjacent blocks in the middle crust reflects a rotational angle ranging from ~80 to 90° in the east to ~110° in the center and west within the WTR (Figure 4d). These values match exceptionally well with paleomagnetic data, which suggest a ~70–110° rotational angle that seems to increase westward within the block (e.g., Hillhouse, 2010; Hornafius et al., 1986; Luyendyk, 1991).

The SAF is commonly regarded as the Pacific-North America plate boundary that absorbed ~75% of the transform motion (Argus et al., 2011). Our model reveals distinct *P*-wave anisotropic features across the SAF (Figure 4). This feature is less clear in the SWS results (Boness & Zoback, 2006; Li & Peng, 2017), possibly because the SWS measurements mainly reflect shallow structures with prevailing microcracks aligned in response to the current N-S compression, in comparison to the middle crust where paleofabrics dominate. The relatively uniform azimuthal anisotropy in the blocks east of the SAF in our model may indicate a simpler evolution with much less rotational history as compared to the western blocks, consistent with tectonic reconstruction (e.g., McQuarrie & Wernicke, 2005). Distinct seismic velocities and anisotropies across the SAF may further imply a contrast of lithological strength that has helped in localizing the SAF (Audet, 2015; Wang et al., 2020). North of the GF, the Sierra Nevada shows similar fast axes to the SB and WPR in the middle crust (Figures 4g and 4h), possibly

reflecting the same tectonic origin of these blocks as a continuous magmatic arc formed during the long-lived Farallon subduction (e.g., Saleeby, 2003).

Further to the south, the ST likely represents a region with seismic anisotropy fully controlled by the present-day deformation. The rapid change of N-S oriented stress-controlled anisotropy in the shallow crust (<6 km) to NE-SW fast axes in the middle crust (~9 km; considering a crustal thickness of ~20 km beneath the ST (Tape et al., 2012)) may stem from aligned fluid-filled secondary faults associated with a series of small block rotations, which are largely governed by distributed dextral shear between the SAF and SJF (Brothers et al., 2009; Liu et al., 2022). At greater depths (>12 km), NW-SE oriented fast axes correspond to a layer of newly underplated gabbroic rocks with possible partial melts (up to 4.5%) organized in anastomosing dikes/veins that are parallel to the shear direction (Barak et al., 2015). This could potentially explain the orientation and large amplitude of the observed azimuthal anisotropy in the lower crust of ST (Figures 4e and 4f), in agreement with teleseismic SWS measurements (Barak & Klemperer, 2016) and a larger-scale surface wave anisotropic tomography (Lin et al., 2011). We note that the NW-SE fast orientations can be observed further to the west beneath parts of the EPR (Figure 4f), matching the spatial extent of the middle to lower crust high velocities (Figures 3e and 3f). This may indicate that the lower crust of the relatively cold Peninsular Ranges has been progressively altered by the hot upwelling upper mantle beneath the ST from the east, as also supported by a significantly thinned (<70 km) lithosphere (Lekic et al., 2011) and a gradually shallowing Moho from the EPR to ST (Yan & Clayton, 2007).

5. Conclusions

We construct a new high-resolution azimuthally anisotropic *P*-wave velocity model of the upper to middle crust beneath southern California using a novel adjoint-state traveltime tomography method. Our model reveals complex anisotropy variations between tectonic blocks at different depths, which are jointly shaped by the present and past plate boundary deformation. We find that seismic anisotropies in the shallow crust (<~6 km) are mainly controlled by the preferred alignment of cracks in response to regional stress. At deeper depths, deviations of fast *P*-wave axes from the $S_{H\max}$ direction suggest a change from crack-to mineral-induced anisotropy, with fast directions mainly reflecting paleofabrics formed during the long-lived Farallon subduction and later extension, except for the ST where significant recent crustal reworkings are found. We observe distinct fast orientations beneath the WTR that are probably generated by its large-scale clockwise rotation. The ~80–110° rotational angle predicted by the fast axis differences from the neighboring blocks is strongly consistent with paleomagnetic data and tectonic reconstructions.

Data Availability Statement

Seismic data used in this study were provided by the Southern California Earthquake Data Center (SCEDC, 2013) (https://scedc.caltech.edu/). The final velocity model can be accessed via https://doi.org/10.21979/N9/JQDOAQ.

Acknowledgments
This study was funded by the National Research Foundation Singapore and the Singapore Ministry of Education under the Research Centers of Excellence Initiative (04MNS001913A620 and 04MNS001953A620). PT is supported by MOE AcRF Tier-2 (MOE2019-T2-2-112) and Tier-1 Grant (RG118/19S). CJ acknowledges the support from an Australian Research Council Discovery Early Career Researcher Award (DE220100907). We thank the helpful discussion with Haibin Yang and the insightful suggestions from Editor Lucy Flesch and two anonymous reviewers. This work comprises Earth Observatory of Singapore contribution no. 448.

References

Almqvist, B. S. G., & Mainprice, D. (2017). Seismic properties and anisotropy of the continental crust: Predictions based on mineral texture and rock microstructure. *Reviews of Geophysics*, *55*(2), 367–433. https://doi.org/10.1002/2016rg000552

Argus, D. F., Gordon, R. G., & DeMets, C. (2011). Geologically current motion of 56 plates relative to the no-net-rotation reference frame. *Geochemistry, Geophysics, Geosystems*, *12*(11), Q11001. https://doi.org/10.1029/2011gc003751

Atwater, T. (1970). Implications of plate tectonics for the cenozoic tectonic evolution of western north America. *The Geological Society of America Bulletin*, *81*(12), 3513–3536. https://doi.org/10.1130/0016-7606(1970)81[3513:Ioptft]2.0.Co;2

Audet, P. (2015). Layered crustal anisotropy around the San Andreas fault near Parkfield, California. *Journal of Geophysical Research: Solid Earth*, *120*, 3527–3543. https://doi.org/10.1002/2014jb011821

Bao, X., Guo, L., & Shen, Y. (2021). Compositional variation in the crust of peninsular ranges and surrounding regions, Southern California, revealed by full-wave seismic and gravity joint inversion. *Journal of Geophysical Research: Solid Earth*, *126*, e2021JB022723. https://doi.org/10.1029/2021jb022723

Barak, S., & Klemperer, S. L. (2016). Rapid variation in upper-mantle rheology across the San Andreas fault system and Salton Trough, southernmost California, USA. *Geology*, *44*(7), 575–578. https://doi.org/10.1130/g37847.1

Barak, S., Klemperer, S. L., & Lawrence, J. F. (2015). San Andreas Fault dip, Peninsular Ranges mafic lower crust and partial melt in the Salton Trough, Southern California, from ambient-noise tomography. *Geochemistry, Geophysics, Geosystems*, *16*(11), 3946–3972. https://doi.org/10.1002/2015gc005970

Barruol, G., & Mainprice, D. (1993). A quantitative evaluation of the contribution of crustal rocks to the shear-wave splitting of teleseismic SKS waves. *Physics of the Earth and Planetary Interiors*, *78*(3–4), 281–300. https://doi.org/10.1016/0031-9201(93)90161-2

Ben-Zion, Y., & Zaliapin, I. (2019). Spatial variations of rock damage production by earthquakes in southern California. *Earth and Planetary Science Letters*, *512*, 184–193. https://doi.org/10.1016/j.epsl.2019.02.006

Berg, E. M., Lin, F. C., Allam, A., Qiu, H., Shen, W., & Ben-Zion, Y. (2018). Tomography of Southern California via Bayesian joint inversion of Rayleigh wave ellipticity and phase velocity from ambient noise cross-correlations. *Journal of Geophysical Research: Solid Earth*, *123*, 9933–9949. https://doi.org/10.1029/2018jb016269

Bernard, R. E., & Behr, W. M. (2017). Fabric heterogeneity in the Mojave lower crust and lithospheric mantle in Southern California. *Journal of Geophysical Research: Solid Earth*, *122*, 5000–5025. https://doi.org/10.1002/2017jb014280

Bird, P. (2003). An updated digital model of plate boundaries. *Geochemistry, Geophysics, Geosystems*, *4*(3), 1027. https://doi.org/10.1029/2001gc000252

Boness, N. L., & Zoback, M. D. (2006). Mapping stress and structurally controlled crustal shear velocity anisotropy in California. *Geology*, *34*(10), 825. https://doi.org/10.1130/g22309.1

Brothers, D. S., Driscoll, N. W., Kent, G. M., Harding, A. J., Babcock, J. M., & Baskin, R. L. (2009). Tectonic evolution of the Salton Sea inferred from seismic reflection data. *Nature Geoscience*, *2*(8), 581–584. https://doi.org/10.1038/ngeo590

Crampin, S. (1987). Geological and industrial implications of extensive-dilatancy anisotropy. *Nature*, *328*(6130), 491–496. https://doi.org/10.1038/328491a0

Dokka, R. K., & Travis, C. J. (1990). Late cenozoic strike-slip faulting in the Mojave Desert, California. *Tectonics*, *9*(2), 311–340. https://doi.org/10.1029/TC009i002p00311

Hadley, D., & Kanamori, H. (1977). Seismic structure of the Transverse ranges, California. *The Geological Society of America Bulletin*, *88*(10), 1469. https://doi.org/10.1130/0016-7606(1977)88<1469:Ssottr>2.0.Co;2

Han, L., Hole, J. A., Stock, J. M., Fuis, G. S., Kell, A., Driscoll, N. W., et al. (2016). Continental rupture and the creation of new crust in the Salton Trough rift, Southern California and northern Mexico: Results from the Salton seismic imaging project. *Journal of Geophysical Research: Solid Earth*, *121*, 7469–7489. https://doi.org/10.1002/2016jb013139

Hauksson, E., Yang, W., & Shearer, P. M. (2012). Waveform relocated earthquake catalog for Southern California (1981 to June 2011). *Bulletin of the Seismological Society of America*, *102*(5), 2239–2244. https://doi.org/10.1785/0120120010

Hillhouse, J. W. (2010). Clockwise rotation and implications for northward drift of the western Transverse ranges from paleomagnetism of the Piuma Member, sespe formation, near Malibu, California. *Geochemistry, Geophysics, Geosystems*, *11*(7), Q07005. https://doi.org/10.1029/2010gc003047

Hornafius, J. S., Luyendyk, B. P., Terres, R. R., & Kamerling, M. J. (1986). Timing and extent of Neogene tectonic rotation in the western Transverse Ranges, California. *GSA Bulletin*, *97*(12), 1476–1487. https://doi.org/10.1130/0016-7606(1986)97<1476:Taeont>2.0.Co2

Jennings, C. W. (1994). *Fault activity map of California and adjacent areas: Sacramento*. scale 1:750000, 1 sheet. California Division of Mines and Geology.

Lee, E. J., Chen, P., Jordan, T. H., Maechling, P. B., Denolle, M. A. M., & Beroza, G. C. (2014). Full-3-D tomography for crustal structure in Southern California based on the scattering-integral and the adjoint-wavefield methods. *Journal of Geophysical Research: Solid Earth*, *119*, 6421–6451. https://doi.org/10.1002/2014jb011346

Lekic, V., French, S. W., & Fischer, K. M. (2011). Lithospheric thinning beneath rifted regions of Southern California. *Science*, *334*(6057), 783–787. https://doi.org/10.1126/science.1208898

Li, Z., & Peng, Z. (2017). Stress- and Structure-Induced anisotropy in southern California from two decades of shear wave splitting measurements. *Geophysical Research Letters*, *44*(19), 9607–9614. https://doi.org/10.1002/2017gl075163

Lin, F.-C., Ritzwoller, M. H., & Snieder, R. (2009). Eikonal tomography: Surface wave tomography by phase front tracking across a regional broad-band seismic array. *Geophysical Journal International*, *177*(3), 1091–1110. https://doi.org/10.1111/j.1365-246X.2009.04105.x

Lin, F.-C., Ritzwoller, M. H., Yang, Y., Moschetti, M. P., & Fouch, M. J. (2011). Complex and variable crustal and uppermost mantle seismic anisotropy in the western United States. *Nature Geoscience*, *4*(1), 55–61. https://doi.org/10.1038/ngeo1036

Liu, Y., Wu, S., & Tong, P. (2022). Depth-dependent crustal azimuthal anisotropy in the Salton Trough, Southern California. *Tectonophysics*, 826. https://doi.org/10.1016/j.tecto.2022.229264

Luyendyk, B. P. (1991). A model for Neogene crustal rotations, transtension, and transpression in southern California. *The Geological Society of America Bulletin*, *103*(11), 1528–1536. https://doi.org/10.1130/0016-7606(1991)103<1528:Amfncr>2.3.Co;2

McQuarrie, N., & Wernicke, B. P. (2005). An animated tectonic reconstruction of southwestern North America since 36 Ma. *Geosphere*, *1*(3), 147–172. https://doi.org/10.1130/GES00016.1

Nicholson, C., Sorlien, C. C., Atwater, T., Crowell, J. C., & Luyendyk, B. P. (1994). Microplate capture, rotation of the western Transverse Ranges, and initiation of the San Andreas transform as a low-angle fault system. *Geology*, *22*(6), 491–495. https://doi.org/10.1130/0091-7613(1994)022<0491:Mcrotw>2.3.Co;2

Porter, R., Zandt, G., & McQuarrie, N. (2011). Pervasive lower-crustal seismic anisotropy in Southern California: Evidence for underplated schists and active tectonics. *Lithosphere*, *3*(3), 201–220. https://doi.org/10.1130/l126.1

Qian, J., Zhang, Y.-T., & Zhao, H.-K. (2007). A fast sweeping method for static convex Hamilton–Jacobi equations. *Journal of Scientific Computing*, *31*(1–2), 237–271. https://doi.org/10.1007/s10915-006-9124-6

Rasolofosaon, P. N. J., Rabbel, W., Siegesmund, S., & Vollbrecht, A. (2000). Characterization of crack distribution: Fabric analysis versus ultrasonic inversion. *Geophysical Journal International*, *141*(2), 413–424. https://doi.org/10.1046/j.1365-246x.2000.00093.x

Saleeby, J. (2003). Segmentation of the laramide slab—Evidence from the southern Sierra Nevada region. *The Geological Society of America Bulletin*, *115*, 655–668. https://doi.org/10.1130/0016-7606(2003)115<0655:Sotlsf>2.0.Co;2

Savage, M. K. (1999). Seismic anisotropy and mantle deformation: What have we learned from shear wave splitting? *Reviews of Geophysics*, *37*(1), 65–106. https://doi.org/10.1029/98rg02075

SCEDC. (2013). Southern California earthquake data center. Dataset. *Caltech*. https://doi.org/10.7909/C3WD3xH1

Schulte-Pelkum, V., Becker, T. W., Behr, W. M., & Miller, M. S. (2021). Tectonic inheritance during plate boundary evolution in Southern California constrained from Seismic anisotropy. *Geochemistry, Geophysics, Geosystems*, *22*(11), e2021GC010099. https://doi.org/10.1029/2021gc010099

Schulte-Pelkum, V., Ross, Z. E., Mueller, K., & Ben-Zion, Y. (2020). Tectonic inheritance with dipping faults and deformation fabric in the brittle and ductile southern California Crust. *Journal of Geophysical Research: Solid Earth*, *125*(8), e2020JB019525. https://doi.org/10.1029/2020jb019525

Shaw, J. H., Plesch, A., Tape, C., Suess, M. P., Jordan, T. H., Ely, G., et al. (2015). Unified structural representation of the southern California crust and upper mantle. *Earth and Planetary Science Letters*, *415*, 1–15. https://doi.org/10.1016/j.epsl.2015.01.016

Tape, C., Liu, Q., Maggi, A., & Tromp, J. (2009). Adjoint tomography of the southern California crust. *Science*, *325*(5943), 988–992. https://doi.org/10.1126/science.1175298

Tape, C., Plesch, A., Shaw, J. H., & Gilbert, H. (2012). Estimating a continuous moho surface for the California unified velocity model. *Seismological Research Letters*, *83*(4), 728–735. https://doi.org/10.1785/0220110118

Tong, P. (2021). Adjoint-State traveltime tomography for azimuthally anisotropic media and insight into the crustal structure of central California near Parkfield. *Journal of Geophysical Research: Solid Earth*, *126*, e2021JB022365. https://doi.org/10.1029/2021jb022365

Tong, P., Yang, D., & Huang, X. (2019). Multiple-grid model parametrization for seismic tomography with application to the San Jacinto fault zone. *Geophysical Journal International*, *218*(1), 200–223. https://doi.org/10.1093/gji/ggz151

Tong, P., Yao, J., Liu, Q., Li, T., Wang, K., Liu, S., et al. (2021). Crustal rotation and fluids: Factors for the 2019 Ridgecrest earthquake sequence? *Geophysical Research Letters*, *48*(3), e2020GL090853. https://doi.org/10.1029/2020gl090853

Wang, K., Jiang, C., Yang, Y., Schulte-Pelkum, V., & Liu, Q. (2020). Crustal deformation in southern California constrained by radial anisotropy from ambient noise adjoint tomography. *Geophysical Research Letters*, *47*(12), e2020GL088580. https://doi.org/10.1029/2020gl088580

Wang, Y. (2014). Seismic ray tracing in anisotropic media: A modified Newton algorithm for solving highly nonlinear systems. *Geophysics*, *79*(1), T1–T7. https://doi.org/10.1190/geo2013-0110.1

Wu, S., Li, T., Wang, D., & Tong, P. (2022). Lower crust structures and dynamics of southern California revealed by first P and PmP traveltime data. *Tectonophysics*, *830*, 229328. https://doi.org/10.1016/j.tecto.2022.229328

Yan, Z., & Clayton, R. W. (2007). Regional mapping of the crustal structure in southern California from receiver functions. *Journal of Geophysical Research*, *112*, B05311. https://doi.org/10.1029/2006jb004622

Yang, W., & Hauksson, E. (2013). The tectonic crustal stress field and style of faulting along the Pacific North America Plate boundary in Southern California. *Geophysical Journal International*, *194*(1), 100–117. https://doi.org/10.1093/gji/ggt113

Yu, Y., & Zhao, D. (2018). Lithospheric deformation and asthenospheric flow associated with the Isabella anomaly in Southern California. *Journal of Geophysical Research: Solid Earth*, *123*, 8842–8857. https://doi.org/10.1029/2018jb015873

Zhao, D., Yu, S., & Liu, X. (2016). Seismic anisotropy tomography: New insight into subduction dynamics. *Gondwana Research*, *33*, 24–43. https://doi.org/10.1016/j.gr.2015.05.008

Zigone, D., Ben-Zion, Y., Campillo, M., & Roux, P. (2015). Seismic tomography of the Southern California plate boundary region from noise-based Rayleigh and love waves. *Pure and Applied Geophysics*, *172*(5), 1007–1032. https://doi.org/10.1007/s00024-014-0872-1